Conformation of the Diphtheria Toxin T Domain in Membranes: A Site-Directed Spin-Labeling Study of the TH8 Helix and TL5 Loop†

Kyoung Joon Oh,‡,§ Hangjun Zhan,||,⊥ Can Cui,|| Christian Altenbach,‡ Wayne L. Hubbell,*,‡ and R. John Collier*,||

Jules Stein Eye Institute and Department of Chemistry and Biochemistry, University of California Los Angeles, Los Angeles, California 90095-7008, and Department of Microbiology and Molecular Genetics, Harvard Medical School, 200 Longwood Avenue, Boston, Massachusetts 02115

Received March 5, 1999; Revised Manuscript Received June 2, 1999

ABSTRACT: The isolated T domain of diphtheria toxin was mutated by cysteine-scanning mutagenesis at 28 consecutive sites (residues 328−355) that comprise the TH8 helix and the TL5 interhelical loop in the native toxin. After derivatizing the mutant proteins with a sulfhydryl-selective nitroxide reagent, we examined the mobility of each nitroxide and its accessibility to polar and nonpolar paramagnetic reagents, before and after insertion into phospholipid bilayers. The data obtained with the proteins in solution at pH 8 are generally consistent with predictions from the crystal structure of the toxin. Upon membrane binding at pH 4.6, a major structural reorganization of the domain was seen, which dramatically reduced the accessibility of most residues in this region to the polar reagent nickel(II)−ethylenediaminediacetate complex (NiEDDA). Many of these residues also showed reduced accessibility to the nonpolar reagent O_2. Periodic accessibility of the nitroxide side chains along the sequence to these reagents shows that TH8 remains largely helical in the membrane-bound state, with one surface associated with protein and the other facing the hydrophobic interior of the bilayer. In addition, the TL5 loop also appears to become α-helical in the membrane, with one surface in contact with protein and the other in contact with the bilayer interior. These findings provide a structural framework for understanding how the T domain forms a transmembrane channel and mediates translocation of diphtheria toxin's enzymic moiety across a membrane.

Diphtheria toxin (DT)[1] (*1*−*3*) belongs to a class of toxic proteins that act by enzymically modifying cytosolic substrates within eukaryotic cells (*4*). The process by which the catalytic moiety is transferred across a membrane to enter the cytosol is not understood for any such toxin. For DT, translocation occurs only after the toxin has bound to its receptor at the cell surface and been delivered by receptor-mediated endocytosis to the endosomal compartment (*5*, *6*). Under the influence of the low pH within that compartment, the toxin undergoes a conformational rearrangement that causes its transmembrane (T) domain to insert into the endosomal membrane (*7*−*13*). This insertion event induces the toxin's catalytic domain to cross the membrane to the cytosolic compartment (*14*−*18*), where it catalyzes the ADP-ribosylation of elongation factor 2, causing inhibition of protein synthesis and cell death (*19*, *20*).

The T domain (Figure 1), situated between the toxin's N-terminal catalytic and C-terminal receptor-binding domains, is composed of 10 α-helices (*24*−*26*). Two long hydrophobic helices, TH8 and TH9, form the core of the T domain and are covered by two other "layers" of helices (*26*). Both the holotoxin and the isolated T domain form voltage-dependent channels in planar bilayers at low pH (pH ∼ 5) (*27*). A T domain fragment, consisting of TH8, TH9, and the interhelical TL5 loop, is apparently sufficient for channel formation (*28*), and various mutations in TL5 and TH9 have been shown to have a major effect on channel formation and toxicity (*26*, *29*−*32*). These results imply that the DT channel is formed by insertion of this helical hairpin into the membrane (*16*, *25*, *26*, *33*−*38*).

The method of site-directed spin labeling (SDSL) has emerged as a powerful tool to probe the structure of proteins both in solution and in membranes (*39*, *40*). In earlier studies, we applied SDSL to the TH9 helix of the T domain and showed that TH9 retains its helicity upon membrane binding (*21*). Here we extend the SDSL studies in the hairpin to cover the TH8 helix and the TL5 interconnecting loop (Figure 1). The data indicate that most of TH8 retains its helicity after binding of T domain to membranes at low pH and that the

† This work was supported by NIH Grants AI-22021 (R.J.C.) and EY-05216 (W.L.H.) and by the Jules Stein Professor Endowment (W.L.H.).

* To whom correspondence should be addressed: phone (*617*) 432-1930; fax (*617*) 432-0115; e-mail jcollier@hms.harvard.edu.

‡ University of California Los Angeles.

§ Present address: Department of Microbiology and Molecular Genetics, Harvard Medical School, 200 Longwood Ave., Boston, MA 02115.

|| Harvard Medical School.

⊥ Present address: Arris Pharmaceutical Corp., 385 Oyster Point Blvd., Suite 3, South San Francisco, CA 94080.

[1] Abbreviations: DT, diphtheria toxin; DTT, dithiothreitol; EPR, electron paramagnetic resonance; GST, glutathione S-transferase; IPTG, isopropyl β-D-thiogalactopyranoside; LUV, large unilamellar vesicle; MTS, methanethiosulfonate; NiEDDA, nickel(II)-ethylenediaminediacetate complex; PCR, polymerase chain reaction; POPC, 1-palmitoyl-2-oleoyl-*sn*-glycero-3-phosphocholine; POPG, 1-palmitoyl-2-oleoyl-*sn*-glycero-3-[phospho-*rac*-(1-glycerol)] (sodium salt); SDSL, site-directed spin labeling.

10.1021/bi990520a CCC: $18.00
Published on Web 07/27/1999

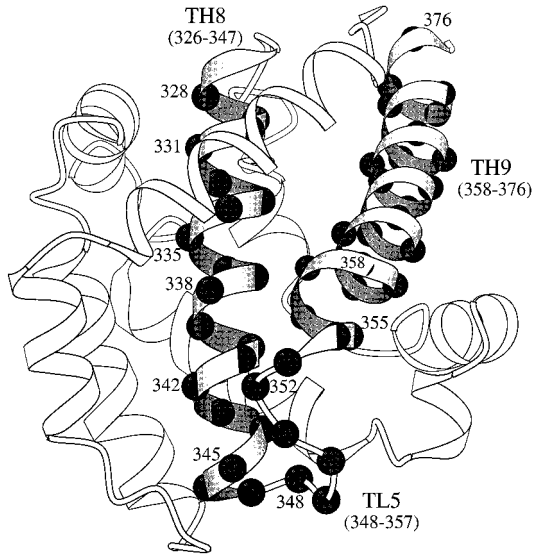

FIGURE 1: Structure of the diphtheria toxin T domain (residues 202−378). The locations of 28 residues (residues 328−355), selected for mutation to cysteine and attachment of spin labels, are identified by large black spheres. The locations of residues spin-labeled in previous studies (*21*, *22*) are shown as small black spheres. The numbering of the mutant residues is that of the native DT. This Molscript representation (*23*) was generated from the coordinates of diphtheria toxin provided by M. J. Bennett and D. Eisenberg (*24*).

TL5 loop is converted into a new helical structure under these conditions.

MATERIALS AND METHODS

Expression of the T Domain as a Hexahistidine-Tagged Fusion Protein. Twenty-eight T domain mutants with a single-cysteine substitution were prepared according to the procedures described earlier (*34*, *41*; see Figure 1) or by an alternative method described below. Briefly, the expression host, *Escherichia coli* BL21(DE3) strain, was transformed with pET15b expression vectors (Novagen) harboring genes for single-cysteine T domain mutants with an N-terminal hexahistidine tail. The T domain was expressed by induction with IPTG and purified with a Ni^{2+} affinity column, and the N-terminal hexahistidine tail was cleaved with thrombin. The T domain mutants prepared this way have four additional residues at the N-terminus: Gly-Ser-His-Met. Purified T domains were stored at −80 °C in the presence of DTT (5−10 mM). All the cysteine mutants used in this study, except S336C[2] and M339C, were prepared by the method described above.

Expression of the T Domain as a Fusion to Glutathione S-Transferase. We made new single-cysteine substitution mutants S336C and M339C using an alternative procedure due to additional mutations found in the above pET15b constructs of the mutants. The T domain was cloned into the pGEX-4T-1 vector (Amersham Pharmacia), which results in the T domain fused to the C-terminal end of glutathione S-transferase. Briefly, a DNA fragment encoding the T domain (residues 202−378 of DT) was amplified by PCR reactions with the following two primers containing *Bam*HI and *Eco*RI restriction sites (boldface), respectively: 5′-CCG CGC **GGA TCC** CAT ATG ATA AAT CTT GAT TGG and 5′-GTC TTC AA**G AAT TC**A TCA GGG ACG. The template for the PCR reaction was pET15b−T (*41*). The amplified DNA fragments were digested with restriction enzymes *Bam*HI and *Eco*RI and purified by agarose gel electrophoresis. The resulting DNA fragments were ligated into pGEX-4T-1 vector (Amersham Pharmacia) by use of the two restriction sites. The ligated plasmids were introduced into *E. coli* XL1 Blue competent cells. The plasmid containing the T domain gene was isolated and subjected to sequencing to verify the nucleotide sequence of the entire T domain gene and its junctions. The resulting pGEX vector harboring the T domain gene was designated as pGT. Mutants S336C and M339C were prepared from pGT by replacing the DNA fragment flanked between *Cla*I and *Eco*RI restriction sites with the corresponding fragments in pET15b-T mutant plasmids. The DNA fragments in the original pET15b-T plasmids coding for these mutants did not have any error in the sequence between the two restriction sites. The entire sequences of the mutant T domain genes and their junctions were verified by sequencing for the two single cysteine mutants.

Plasmids prepared as described above were used to transform *E. coli* BL21, and the T domain mutants were expressed cytoplasmically as a fusion protein to GST. Briefly, protein expression was induced in cultures of $A_{600} \sim 1.0$ by adding IPTG to a final concentration of 1 mM. After 1 h at 37 °C or 2 h at 28 °C, cells were harvested by centrifugation and stored at −20 °C. Typically, cell pellets from 4 L were thawed and resuspended in ∼40 mL of phosphate-buffered saline (140 mM NaCl, 2.7 mM KCl, 10 mM Na_2HPO_4, and 1.8 mM KH_2PO_4) by brief sonication. The cells were disrupted by French press. Cell debris was removed by centrifugation at 12000*g* for 20 min at 4 °C. The supernatant was filtered through a 0.2 μm filter and loaded onto a column packed with 2 mL of glutathione−Sepharose 4B (Amersham Pharmacia), which was prepared according to the manufacturer's manual. After the column was washed with 10 bed volumes of phosphate-buffered saline, the GST−T fusion protein was eluted with 5 bed volumes of 10 mM glutathione in 50 mM Tris-HCl, pH 8.0, in 1 mL fractions. The fractions containing the protein were combined and concentrated with a centrifugal concentrator Centriprep-10 (Amicon). The GST−T fusion protein was cleaved by treating the fusion protein with thrombin protease (Novagen) for 8 h at room temperature. The T domain was separated from the GST on a column packed with glutathione−Sepharose 4B (Amersham Pharmacia) by eluting with phosphate-buffered saline. Collected T domain fractions were concentrated by centrifugal concentrator. T domains were stored at −80 °C in the presence of 15% (v/v) glycerol and 5−10 mM DTT. The T domain mutants prepared this way also have four additional residues at the N-terminus: Gly-Ser-His-Met.

Spin Labeling of the Monomer and Dimer Fractions of T Domain Cysteine Mutants. T domain cysteine mutants were purified by gel-filtration chromatography (Superdex75, Amersham Pharmacia), eluting with 20 mM Tris (pH 8), 150 mM NaCl, 1 mM EDTA, and 0.02% (w/v) NaN_3 (buffer A). Immediately following purification, fractions containing T domain were reacted for 16 h at room temperature with a

[2] To designate the amino acid substitution mutants, we specify, in order, the original residue, the sequence position, and the substituted residue. For example, S336C is a mutant in which the serine at 336 was replaced by cysteine.

10-fold excess of spin label (I) to generate the spin-labeled side chain designated as R1 (Figure 2). Unreacted spin label was removed by gel-filtration chromatography (Superdex 75) or, in the case of small samples, by dialysis against buffer A. The labeled protein was concentrated with a Microsep centrifugal concentrator (Filtron Technology Corp., Northborough, MA), and the final concentration was determined by a modified Lowry assay (*42*) with bovine serum albumin as standard. The molecular weight of the T domain was estimated by gel filtration (Superdex 75).

Preparation of LUVs and Membrane-Bound T Domain. POPG (20 mg) and POPC (100 mg) (both from Avanti, Birmingham, AL) were suspended in 1.2 mL of 100 mM sodium acetate buffer, pH 4.6, and vortexed briefly. The lipid suspension was subjected to 5 cycles of freezing and thawing. LUVs were prepared by extruding the resulting multilamellar vesicles 10−15 times through two sheets of polycarbonate membrane with pores 100 nm in diameter (43, Avestin, Ottawa, Canada).

Membrane-bound T domain was prepared as described (*41*). Briefly, the pH of the LUV suspension was raised to pH 7−8 with 1 N NaOH just prior to protein addition. T domain was added to the vesicles with an approximate 1:500 molar ratio of protein to phospholipid. To induce binding, a predetermined amount of 100 mM sodium acetate solution was slowly added to the protein−vesicle mixture to a final pH of 4.6. The binding was allowed to proceed for about 30 min. The membrane-bound T domain was pelleted by centrifugation at 15000*g* for 3 min at room temperature.

In two cases, A330R1 and A334R1, the soluble protein precipitated during the spin-labeling reaction, and labeling was carried out in the membrane-bound state. For this purpose, the proteins were allowed to bind to the vesicles as described above. The pH of the protein−vesicle aggregates were then brought back to pH ∼ 6.5 by addition of NaOH. Equimolar spin label was added to the solution and allowed to react overnight at room temperature. The protein−vesicle mixture was washed repeatedly through Microcon centrifugal concentrators to remove unreacted spin labels. After washing, the protein−vesicle solution was titrated back to pH 8 or to pH 4.6 for EPR studies.

EPR Measurements and Depth Calibration. Samples were contained in TPX capillaries and EPR spectra were recorded on a Varian E-109 EPR spectrometer fitted with a loop−gap resonator (*44*). Power saturation measurements and data analysis to obtain the accessibility parameters $\Pi(O_2)$ and Π(NiEDDA) were carried out as previously described (*45*). The parameter Φ, defined as

$$\Phi = \ln [\Pi(O_2)/\Pi(\text{NiEDDA})] \quad (1)$$

has been shown to be a linear function of the depth of a nitroxide in the bilayer interior measured from the membrane/aqueous interface (*46*). Thus

$$d = a\Phi + b \quad (2)$$

where d is the depth of immersion in angstroms. To determine the constants a and b for bilayers containing POPC, POPG, and bound T domain in a 415:85:1 molar ratio at pH = 4.6, Φ values were obtained for nitroxides positioned at known depths in the bilayer on the 2-acyl chain of phosphatidylcholine spin labels. For this purpose, 7-doxyl, 10-doxyl, and 12-doxyl phosphatidylcholines were employed (Avati Polar Lipids, Birmingham, AL), the nitroxides of which reside at estimated depths of 10.5, 14, and 16 Å, respectively (*45*).

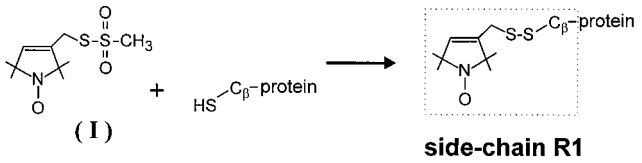

FIGURE 2: Reaction of spin label (**I**) to generate nitroxide side chain R1.

In all cases, $\Pi(O_2)$ was obtained at the concentration of O_2 in equilibrium with air at room temperature. For Π(NiEDDA), the NiEDDA concentration was 20 mM, except for depth estimation in the membrane, where 200 mM was used.

RESULTS

Monomeric and Dimeric Forms of T Domain in Solution. Size-exclusion chromatography of wild-type and mutant T domains revealed the existence of two aggregation states in solution at pH 8 (see also ref *41*), with molecular masses estimated to be 25 and 40 kDa. Given the calculated molecular mass of 19.2 kDa for the T domain monomer, we infer that the two states correspond to monomer and dimer. Both forms had the same electrophoretic mobility on SDS−PAGE under reducing or nonreducing conditions, excluding the possibility that dimerization of the Cys-containing mutant forms involves disulfide bond formation.

Spin labels in close proximity within a dimer would have spin−spin interaction, giving rise to a broadening or possibly resolved splittings in the EPR spectrum (*47*−*50*); and a strong spin−spin interaction was in fact detected in the dimer of one mutant, I353R1. Figure 3 shows a comparison of the EPR spectra for the monomer and dimer forms of I353R1, obtained by separately spin-labeling the monomer and dimer fractions obtained from gel filtration. The first-derivative EPR spectrum of the monomer fraction corresponds to that of a single population of a highly mobile nitroxide, whereas the spectrum of the dimer fraction has an additional spectral component with a splitting of ∼105 G arising from strong spin−spin interactions (Figure 3A). The corresponding absorption spectrum (Figure 3B) clearly reveals that the broad component is the dominant population. The sharper component likely arises from a small amount of monomer in equilibrium with the dimer. Interaction strengths of this magnitude require that the interspin distance be on the order of 10 Å or less (*49*; K. J. Oh and W. L. Hubbell, unpublished observation).

In the membrane-bound state, both monomeric and dimeric forms gave essentially identical spectra without indication of strong spin−spin interaction (Figure 3C). This implies that the T domain adopts the same conformation in the membrane regardless of its aggregation state in solution and that the I353R1 residues of the dimer separate during membrane insertion. For most of the mutants, the mixture of monomer and dimer was used for membrane binding studies.

Structure of the Spin-Labeled T Domain in Solution at pH 8. Figure 4 shows the EPR spectra for the R1 side chains in

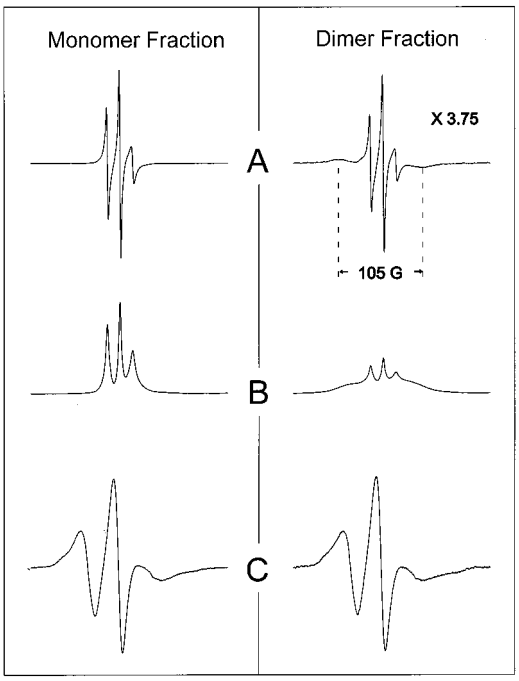

FIGURE 3: EPR spectra of the monomer (left panel) and dimer (right panel) fractions of I353R1 T domain. (A) First-derivative absorption spectra in solution at pH 8.0; (B) absorption spectra in solution at pH 8.0; (C) first-derivative absorption spectra bound to vesicles at pH 4.6. The magnetic field scan range for spectra A and B is 245 G, and for spectra C, 98 G. In spectra A, the vertical gain is 3.75× higher for the dimer relative to the monomer for the same amount of protein.

solution at pH 8 (dotted traces), and Figure 5 shows the corresponding accessibility parameters for O_2 and NiEDDA. Qualitatively, the R1 side chains at residues 328−340 show restricted mobility, judging from the generally well-resolved outer hyperfine extrema, characteristic of sites buried in a protein interior (*51*). The accessibility of R1 residues in this sequence is correspondingly low, except at sites 328 and 335. Residue 328 has slightly higher accessibilities to O_2 and NiEDDA than others in the region, consistent with its partially exposed location at the N-terminal end of the TH8 helix. The nitroxide residue at 335 is expected to be buried in the interior of the protein but apparently has a high solvent accessibility. Moreover, the R1 side chains at 334, 335, and 338 have distinctly higher mobility than others in the 328−340 region, evident in the poorly resolved high-field hyperfine extrema (Figure 4, dotted trace). These three residues are clustered together on one face of the TH8 helix, and the data suggest a more loosely packed structure in this region, although a local perturbation due to the nitroxide at these buried sites is possible.

Spectra for the R1 residue at sites 341−348 are typically multicomponent and may be qualitatively characterized as having intermediate mobility, except at 343 and 344, which are relatively immobilized. As expected, the mobilities are reflected in the accessibilities measured by Π values (Figure 5). Thus R1 at each site in the sequence has partial to high accessibility, except at 343 and 344, which are inaccessible, consistent with their low mobility. These results are in accord with the crystal structure, wherein the sequence 341−348 lies at the C-terminal end of helix TH8, one face of which projects out of the core of the molecule and is exposed to solvent (Figure 1). Residues 342 and 345−348 are all

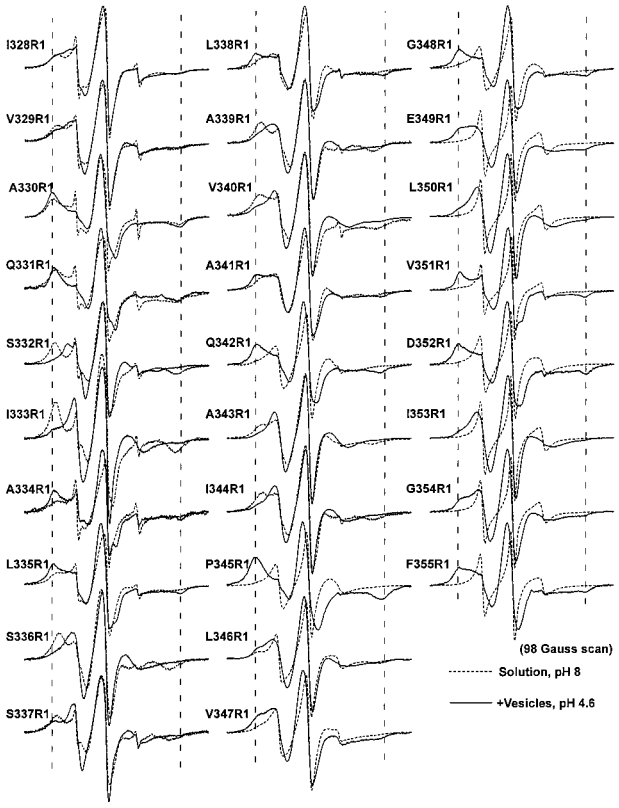

FIGURE 4: EPR spectra[3] of T domain mutants. The dotted traces are the EPR spectra of T domain mutants in solution at pH 8. The solid traces are EPR spectra of T domains bound to 17% POPG/POPC (mol/mol) vesicles at pH 4.6. The vertical dashed lines mark the locations of the largest outer hyperfine extrema.

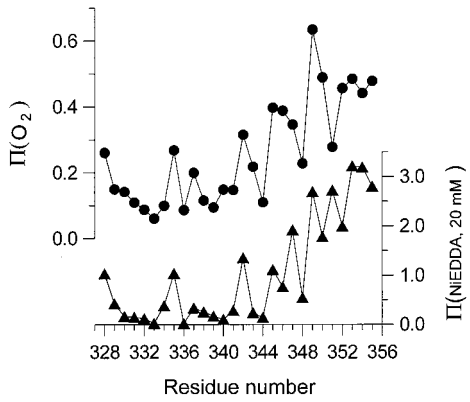

FIGURE 5: Accessibility parameters Π (O_2) and Π(NiEDDA) for R1 residues in the T domain in solution, pH 8.

predicted to have partial solvent exposure, consistent with the experimental accessibility and mobility data. Residues 343 and 344 are buried in the structure, and each is expected to have low mobility and accessibility. The buried residues 343 and 344 are correctly identified by the EPR data.

R1 residues at sites 349−355 have dominant sharp spectral features, indicating high nitroxide mobility (Figure 4), and have high accessibilities, consistent with their location in the solvent-exposed loop structure of TL5 (Figure 5).

A plot of Π(O_2) versus Π(NiEDDA) (Figure 6A) resolves the various residues in the water-soluble protein (solid

[3] The EPR spectra and the accessibility parameters of S332R1 and V351R1 were reported previously (see ref *41*). These were incorporated in this report for the continuity of the data.

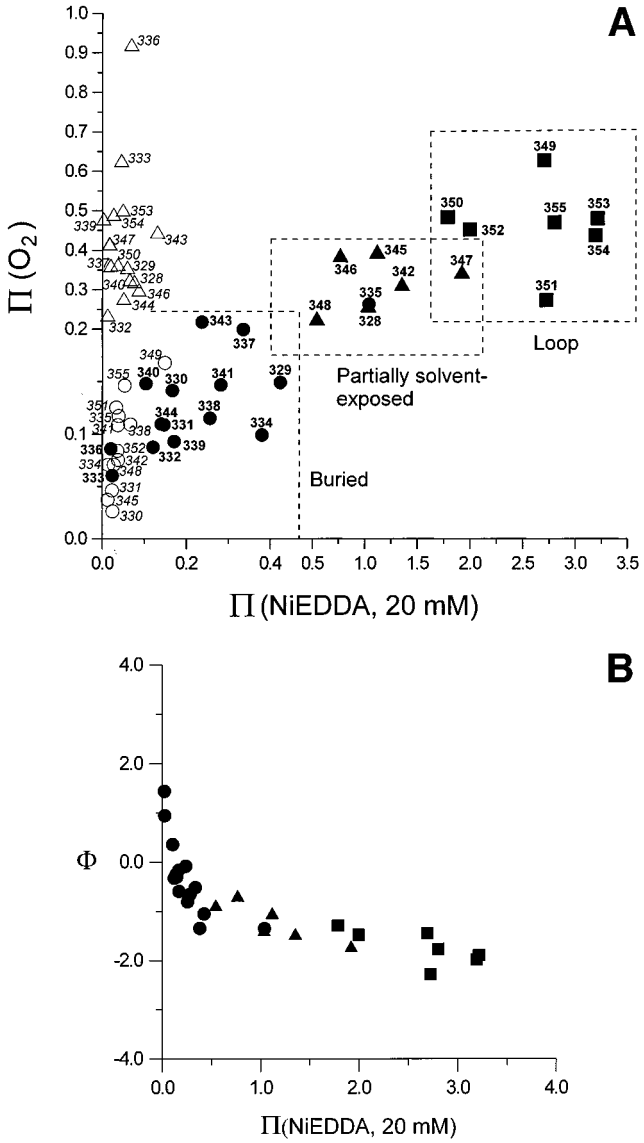

FIGURE 6: (A) Π (O_2) vs Π(NiEDDA) plot for R1 residues in solution state at pH 8 (solid symbols) and in the membrane-bound state, pH 4.6 (open symbols). The shapes of the solid symbols identify the topographical locations of R1 residues predicted from the crystal structure. (●) Buried sites; (▲) partially solvent-exposed sites; (■) loop sites. For open symbols referring to the membrane-bound state, (○) identifies buried sites and (△) lipid-exposed sites. (**B**) Plot of the parameter Φ as a function of residue accessibility measured by Π(NiEDDA).

symbols) into specific topographical domains within the structure and succinctly summarizes the data on accessibility. Thus buried, partially solvent-exposed, and loop residues each cluster together in regions of low, intermediate, and high accessibility, respectively. The overall agreement between the features of the plot and the location of residues in the crystal structure is good, except for 335R1, as noted above.

The contrast parameter $\Phi = \ln [\Pi(O_2)/\Pi(\text{NiEDDA})]$ was introduced earlier as an empirical measure of depth for nitroxides in phospholipid bilayers (*46*). A basic assumption underlying this application is that all sites exposed to a homogeneous medium should have similar values for Φ; that is, both $\Pi(O_2)$ and Π(NiEDDA) should be similar measures of solvent accessibility in a given medium. The data of Figure 6A show that $\Pi(O_2)$ and Π(NiEDDA) are roughly linearly correlated for the T domain in solution, thereby supporting this assumption. Figure 6B analyzes this point in more detail with a plot of Φ as a function of residue accessibility, as measured by Π(NiEDDA). Φ does indeed approach a constant value for the highly exposed loop residues [Π(NiEDDA) ≥ 2] but increases dramatically for more buried sites [Π(NiEDDA) ≤ 0.5]. This is likely due to a size-exclusion effect that limits the diffusion of the larger NiEDDA complex in the protein interior relative to O_2 (*46*). For this reason, only highly solvent-exposed residues are used in the estimation of residue depth in bilayers (see below).

Structure of the Sequence 328−355 in the Membrane-Bound State. A plot of $\Pi(O_2)$ versus Π(NiEDDA) for membrane-bound T domain mutants (open symbols in Figure 6A) shows that most residues experience a dramatic diminution in Π(NiEDDA) in the membrane-bound state relative to the solution form at pH 8. Major changes in $\Pi(O_2)$ as well are seen at many sites. The pattern seen in the membrane-bound T domain consists of two clusters: (i) residues with low accessibility to both O_2 and NiEDDA, identified as buried sites, and (ii) residues with high $\Pi(O_2)$ and low Π(NiEDDA) values, identified as sites directly solvated by the hydrophobic interior of the lipid bilayer (*40*).

Insights into the local secondary structure of the membrane-inserted T domain are obtained by plotting the sequence dependence of accessibility. As shown in Figure 7A, $\Pi(O_2)$ is a periodic function of position throughout the entire sequence, with a period corresponding to that of an α-helix. These data strongly suggest that the α-helical structure of TH8 is conserved in the membrane-bound state and in fact is extended to include residues belonging to the TL5 region of the solution structure (residues 348−355). Note that the residues at $\Pi(O_2)$ maxima (329, 333, 336, 339, 343, 347, 350, and 353) and minima (330, 334, 338, 342, 345, 348, 352, and 355) correspond to the lipid-facing and buried clusters of Figure 6A, respectively (see also Figure 7C,D). This reveals that the helical structure has one face solvated directly by the bilayer, with the opposing face in direct interaction with the other portions of the protein.

The mobilities of the R1 side chains inferred from the line shapes support this interpretation (solid trace in Figure 4). EPR spectral line shapes reflecting immobilized R1 residues, characteristic of buried sites, occur periodically along the sequence every third or fourth residue and correspond to the minima in $\Pi(O_2)$. Figure 7 panels C and D summarize the mobility and accessibility data in the sequence 328−355 on two helical wheel diagrams; one for the TH8 helix sequence (328−347) and the other for the TL5 sequence (348−355). This representation clearly shows the close correspondence between the experimental accessibility and mobility data and a structural model consisting of a regular helix in an asymmetric protein/lipid environment.

For a helix in contact on one face with the lipid bilayer and on the other with protein, all values of Π(NiEDDA) are expected to be very small due to the limited partition of the NiEDDA from the aqueous phase to both buried sites and the membrane interior. The data of Figure 6A, obtained with 20 mM NiEDDA, are clearly in accord with this expectation, and many of the values are near the lower limit of reliable measurement. At 200 mM NiEDDA, values of Π(NiEDDA) are significantly larger and can be reliably determined at most sites (Figure 7A). In the sequence 328−

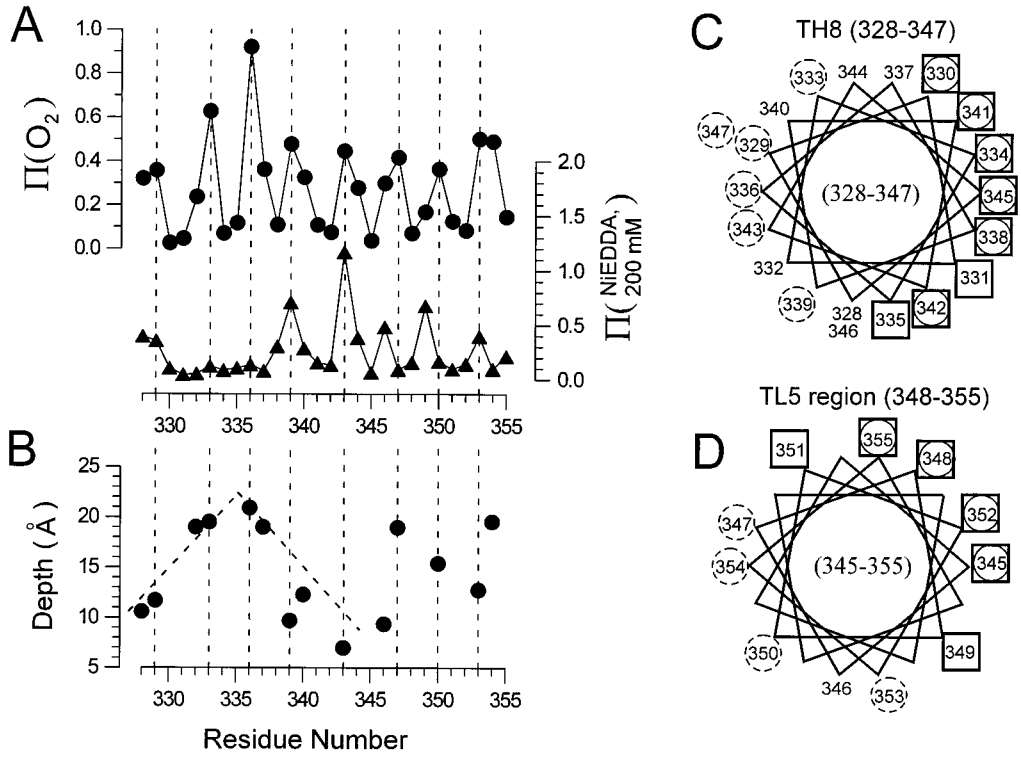

FIGURE 7: (A) Accessibility parameters Π (O_2) and Π(NiEDDA) for R1 residues in the membrane-bound T domain, pH 4.6. (**B**) Immersion depth of R1 chains in the bilayer relative to the membrane/aqueous boundary vs residue number. The immersion depth was calculated from eq 2 with $a = 4.81$ and $b = 11.6$ as determined from the calibration described in Materials and Methods. (**C**, **D**) Helical wheel plots of spin-labeled residues of the TH8 helix sequence and the TL5 sequence, respectively. Squares indicate sites of immobilized residues. Dotted circles and solid circles denote residues at the maxima of Π(O_2) and minima of Π(O_2), respectively. Residues 345−347 are included in both wheels to show the relative positions of these with respect to the other residues.

345, each of the maxima in Π(O_2) (lipid-exposed residues) has a corresponding local maximum in Π(NiEDDA). Beyond this point, there is no clear correlation between Π(NiEDDA) and Π(O_2).

Topography of the Sequence 328−355 in the Membrane. A helix with one surface solvated by the lipid bilayer and the other interacting with protein could, as two extremes, either lie parallel to the bilayer surface or adopt a transmembrane orientation. In principle, these topographies can be distinguished on the basis of the depth of the nitroxide side chains from the membrane−solution interface (*21*). For the parallel orientation, all side chains facing the bilayer would be expected to lie within a narrow depth range. For the transmembrane orientation, the maximum depth occurs near the center of the membrane, and depth decreases as the nitroxide moves away from this position toward either bilayer surface.

Figure 7B shows the depth of immersion calculated for the residues on the lipid-exposed face of the helix (residues marked by the vertical dashed lines in Figure 7A). These are the most highly exposed sites, where steric exclusion of NiEDDA relative to O_2 should be minimal. In addition, we have included sites 328, 332, 337, 340, 346, and 354 in the measurement, because R1 residues at these sites are also relatively exposed, judging from their high mobility and O_2 accessibility. The overall depth profile of the 328−355 region is not consistent with either a continuous transmembrane or a continuous surface-adsorbed helix. For the sequence of 328−343, one sees an apparent increase in depth from 328 to a maximum at residue 336, followed by a decrease in depth to residue 343. From 347 to 354, the depths, however, remain within an approximately 7 Å range centered about a depth of 15 Å.

DISCUSSION

The nitroxide side-chain mobility (Figure 4) and accessibility (Figures 5 and 6A) in the spin-labeled T domain mutants in solution are in excellent agreement with expectations based on the crystal structure of the protein (Figure 1). This result contributes to a growing body of evidence that the R1 nitroxide side chain produces little perturbation of protein structure at the level of the backbone fold (*51*, *52*).

Upon membrane binding, a dramatic reorganization in tertiary structure takes place, as illustrated by the changes in R1 side-chain mobility (Figure 4) and topography (Figure 6A). A striking feature of the membrane-bound state is that all R1 residues in the sequence 328−355 are essentially inaccessible to the polar reagent NiEDDA at 20 mM. Thus, none of the residues is exposed to the aqueous solution in the membrane-bound state, even though half the sites are partially or fully solvated in the solution structure. Low values of Π(NiEDDA) are characteristic of both buried and lipid-exposed sites, due in the latter case to the low solubility of the reagent in the membrane interior. Buried sites can be distinguished from lipid-exposed sites by a second accessibility dimension, Π(O_2), as shown in Figure 6A. Roughly half the sites are found in each category for the membrane-bound T domain.

The secondary structure of the sequence 328−355 appears to be α-helical in the membrane-bound state, but the residue

depth profile (Figure 7B) is not compatible with a single continuous helix. The data may be consistent with a model in which residues 328−355 form two helical segments of different orientation in the membrane. One helical segment includes residues 328−343 in a transmembrane orientation, with residue 336 lying near the center of the bilayer at a depth of about 20 Å from the plane of the lipid phosphate groups. This configuration is supported by the depth profile data (Figure 7B). The heavy dashed lines in Figure 7B are drawn with a slope of 1.5 Å/residue, the expected profile for a transmembrane helix. A more definitive orientation of this helix might be obtained with additional data points upstream of residue 328.

The depth pattern for residues 346−355 is difficult to interpret due to the smaller number of residues suitable for depth determination and the irregular pattern of the depths. One model consistent with the data assumes that residues 347−355 form a second helix, lying more or less parallel to the membrane surface. To be consistent with the maximum depth recorded for residues 347 and 354 (Figure 7B), one surface of the helix containing these residues must lie near the center of the bilayer. Although the opposite surface of the helix would lie near the aqueous interface, it must interact with other portions of the protein, to satisfy the requirement of residue immobility and inaccessibility at that surface (Figure 7D). Presumably, this helical segment would be located on the inner leaflet of the bilayer (opposite to the leaflet from which insertion occurred).

Finally, the overall model for the 328−355 structure is consistent with the pattern of Π(NiEDDA) at 200 mM in the membrane-bound state (Figure 7A). From 328 to 338, Π(NiEDDA) is low but has local maxima that are in phase with those of $\Pi(O_2)$, as expected for sites on a helix that is exposed to a bilayer interior on one side and faces protein on the opposite side. The value of Π(NiEDDA) is very low at 336 due to its depth in the bilayer, and the expected local maximum is not well resolved. The values at 339 and 343 are relatively high, presumably due to their closer location to the membrane surface. In the sequence 344−355, distinct local maxima of Π(NiEDDA) occur periodically at 346, 349, and 353. They are clustered on one side of the helical wheel at the lipid/protein interface, which would be near the membrane/aqueous interface in the putative helical conformation (Figure 7D).

Because proline 345 is critical in the insertion of T domain into bilayers (*53*), mutant P345R1 might have not behaved in our experiments as the wild-type or other mutant forms of T domain. This may invalidate the EPR data for this residue in our study, but our overall conclusions are not affected by omitting data obtained with P345R1.

Our results concerning the conformation of the TH8−TH9 region of DT in the membrane relate to the larger question of the mechanism by which T domain insertion promotes translocation of the C-domain. Senzel et al. (*17*) have shown that the N-terminal region of T domain translocates to the opposite side of the membrane when the isolated domain inserts into and forms a transmembrane channel in planar lipid bilayers. This suggests that the T domain contains the entire molecular machinery for mediating transfer of the C-domain across membrane and that translocation of the N-terminus of the T domain initiates translocation of the enzymic C-domain of the toxin. The structure that the TH8−TH9 region adopts in the membrane may represent the key to understanding the translocation process.

Fluorescence measurements with three, bimane-labeled, single-Cys T domains (with Cys at positions 322, near the amino-terminal end of helix TH8; 333, in helix TH8; and 356, near the amino-terminal end of helix TH9) have shown that the domain can adopt two forms in the membrane—a deep form and a shallow form (*35*). There is increasing preference for the deep form as the bilayer thickness is decreased and the protein-to-lipid ratio is increased (*35*). Also, it has recently been reported that addition of heterologous proteins in a molten globule-like conformation induces transition of T domain from a shallow membrane-inserted form to its deeply inserted form (*18*). The deep form was suggested to be consistent with a transmembrane helical model (*36*, *37*). The average chain length of the lipids in vesicles and the ratio of protein to lipid used in our study are comparable to those conditions in which the majority of T domain was in the deep form (*18*, *35*−*37*). Thus it is likely that the structure described by the SDSL experiments presented here corresponds to the deep form (*18*, *35*−*37*).

Depth estimates from EPR measurements on TH8 reported here and on TH9 reported earlier (*21*, *22*) suggest a transmembrane configuration of this region in our system. Although our data from EPR measurements will be useful in the long term in defining a model of this region in the membrane, many aspects of this structure remain poorly defined, and it would be speculative at this point to propose a specific model. Major unknowns include the following:

(i) The aggregation state of the T domain. There are suggestions from planar bilayer studies that the channel may be unimolecular (*34*). We have not seen any evidence of strong spin−spin interactions in our studies of membrane-bound T domain, but such interactions are only observed when spin labels are within ∼10 Å (*49*). The absence of strong spin−spin interactions, thus, does not necessarily support the monomeric channel.

(ii) Residue−residue contacts. The restricted side-chain mobility observed in certain regions of TH8−TH9 may reflect contacts solely within the TH8−TH9 region but could also involve other regions. If the N-terminus of the T domain is translocated across the membrane to the opposite side of insertion (*17*) and the TH8−TH9 region adopts a transmembrane configuration, with the N-terminus of TH8 and the C-terminus of TH9 at the same side of protein insertion (*36*), at least one additional segment of the protein must cross the membrane. This segment might therefore be involved in contacts with TH8−TH9.

(iii) Residues in contact with the aqueous phase. Channel conductance measurements have been performed in a planar bilayer system with single-cysteine T domains throughout the TH8−TH9 hairpin to determine the accessibility of those residues in the membrane to water-soluble, charged, sulfhydryl-specific methanethiosulfonate reagents (*34*). Conductance changes were seen in large segments of TH8, almost all of TL5, and the amino-terminal region of TH9. However, the nature of the approach does not permit conclusions to be drawn about the accessibility of sites where no conductance change was seen. It is therefore difficult to correlate these results with those of NiEDDA accessibility in EPR measurements.

Although the structure of the TH8−TH9 region in the membrane remains elusive, the recent rapid pace of advances makes it likely that a model consistent with the data from diverse methods will soon emerge.

ACKNOWLEDGMENT

We thank M. J. Bennett and D. Eisenberg for providing the coordinates of the refined DT crystal structure.

REFERENCES

1. Collier, R. J. (1975) *Bacteriol. Rev. 39*, 54−85.
2. Pappenheimer, A. M., Jr. (1977) *Annu. Rev. Biochem. 46*, 69−94.
3. Greenfield, L., Bjorn, M. J., Horn, G., Fong, D., Buck, G. A., Collier, R. J., and Kaplan, D. A. (1983) *Proc. Natl. Acad. Sci. U.S.A. 80*, 6853−6857.
4. Moss, J., Iglewski, B., Vaughan, M., Tu, A. T., Eds. (1995) *Bacterial Toxins and Virulence Factors in Disease: Handbook of Natural Toxins*, Vol. 8, Marcel Dekker, Inc., New York.
5. Morris, R. E., Gerstein, A. S., Bonventre, P. F., and Saelinger, C. B. (1995) *Infec. Immun. 50*, 721−727.
6. Naglich, J. G., Metherall, J. E., Russell, D. W., and Eidels, L. J. (1992) *Cell 69*, 1051−1061.
7. London, E. (1992) *Biochim. Biophys. Acta 1113*, 25−51.
8. Tortorella, D., Sesardic, D., Dawes, C. S., and London, E. (1995) *J. Biol. Chem. 270*, 27446−27452.
9. Cabiaux, V., Quertenmont, P., Conrath, K., Brasseur, R., Capiau, C., and Ruysschaert, J. M. (1994) *Mol. Microbiol. 11*, 43−50.
10. Moskaug, J. O., Stenmark, H., and Olsnes, S. (1991) *J. Biol. Chem. 266*, 2652−2952.
11. Sandvig, K., and Olsnes, S. (1980) *J. Cell Biol. 87*, 828−832.
12. Draper, R. K., and Simon, M. I. (1980) *J. Cell Biol. 87*, 849−854.
13. Kagan, B. L., Finkelstein, A., and Colombini, M. (1981) *Proc. Natl. Acad. Sci. U.S.A. 78*, 4950−4954.
14. Montecucco, C., Papini, E., Schiavo, G., Padovan, E., and Rossetto, O. (1992) *FEMS Microbiol. Immun. 105*, 101−111.
15. Madshus, I. H., Wiedlocha, A., and Sandvig, K. (1994) *J. Biol. Chem. 269*, 4648−4652.
16. O'Keefe, D. O., Cabiaux, V., Choe, S., Eisenberg, D., and Collier, R. J. (1992) *Proc. Natl. Acad. Sci. U.S.A. 89*, 6202−6206.
17. Senzel, L., Huynh, P. D., Jakes, K. S., Collier, R. J., and Finkelstein, A. (1998) *J. Gen. Physiol. 112*, 317−324.
18. Ren, J., Kachel, K., Kim, H., Malenbaum, S. E., Collier, R. J., and Finkelstein, A. (1999) *Science 284*, 955−957.
19. Honjo, T., Nishizuka, Y., and Hayaishi, O. (1968) *J. Biol. Chem. 243*, 3553−3555.
20. Van Ness, B. G., Howard, J. B., and Bodley, J. W. (1980) *J. Biol. Chem. 255*, 10717−10720.
21. Oh, K. J., Zhan, H., Cui, C., Hideg, K., Collier, R. J., and Hubbell, W. L. (1996) *Science 273*, 810−812.
22. Oh, K. J., Altenbach, C., Collier, R. J., and Hubbell, W. L. (1999) *Methods Mol. Biol.* (in press).
23. Kraulis, P. J. (1991) *J. Appl. Crystallogr. 24*, 946−950.
24. Bennett, M. J., and Eisenberg, D. (1994) *Protein Sci. 3*, 1464−1475.
25. Choe, S., Bennett, M. J., Fujii, G., Curmi, P. M., Kantardjieff, K. A., Collier, R. J., and Eisenberg, D. (1992) *Nature 357*, 216−222.
26. Silverman, J. A., Mindell, J. A., Finkelstein, A., Shen, W. H., and Collier, R. J. (1994) *J. Biol. Chem. 269*, 22524−22532.
27. Mindell, J. A., Zhan, H., Huynh, P. D., Collier, R. J., and Finkelstein, A. (1994). *Proc. Natl. Acad. Sci. U.S.A. 91*, 5272−5276.
28. Silverman, J. A., Mindell, J. A., Zhan, H., Finkelstein, A., and Collier, R. J. (1994) *J. Membr. Biol. 137*, 17−28.
29. Falnes, P. O., Madshus, I. H., Sandvig, K., and Olsnes, S. (1992) *J. Biol. Chem. 267*, 12284−12290.
30. Johnson, V. G., Nicholls, P. J., Habig, W. H., and Youle, R. J. (1993) *J. Biol. Chem. 268*, 3514−3519.
31. VanderSpek, J., Cassidy, D., Genbauffe, F., Huynh, P. D., and Murphy, J. R. (1994) *J. Biol. Chem. 269*, 21455−21459.
32. Kaul, P., Silverman, J., Shen, W. H., Blanke, S. R., Huynh, P. D., Finkelstein, A., and Collier, R. J. (1996) *Protein Sci. 5*, 687−692.
33. Mindell, J. A., Silverman, J. A., Collier, R. J., and Finkelstein, A. (1994) *J. Membr. Biol. 137*, 29−44.
34. Huynh, P. D., Cui, C., Zhan, H., Oh, K. J., Collier, R. J., and Finkelstein, A. (1997) *J. Gen. Physiol. 110*, 229−241.
35. Wang, Y., Malenbaum, S. E., Kachel, K., Zhan, H., and Collier, R. J. (1997) *J. Biol. Chem. 272*, 25091−25098.
36. Kachel, K., Ren, J., Collier, R. J., and London, E. (1998) *J. Biol. Chem. 273*, 22950−22956.
37. Malenbaum, S. E., Collier, R. J., and London, E. (1998) *Biochemistry 37*, 17915−17922.
38. Ren, J., Sharpe, J. C., Collier, R. J., and London, E. (1999) *Biochemistry 38*, 976−984.
39. Hubbell, W. L., and Altenbach, C. (1994) in *Membrane Protein Structure: Experimental Approaches* (White, S., Ed.) pp 224−248, Oxford University Press, London.
40. Hubbell, W. L., and Altenbach, C. (1994) *Curr. Opin. Struct. Biol. 4*, 566−573.
41. Zhan, H., Oh, K. J., Shin, Y. K., Hubbell, W. L., and Collier, R. J. (1995) *Biochemistry 34*, 4856−4863.
42. Peterson, G. L. (1977) *Anal. Biochem. 83*, 346−356.
43. Szoka, F., and Papahadjopoulos, D. (1978) *Proc. Natl. Acad. Sci. U.S.A. 75*, 4194−4198.
44. Hubbell, W. L., Froncisz, W., and Hyde, J. S. (1987) *Rev. Sci. Instrum. 58*, 1879−1886.
45. Farahbakhsh, Z. T., Altenbach, C., and Hubbell, W. L. (1992) *Photochem. Photobiol. 56*, 1019−1033.
46. Altenbach, C., Greenhalgh, D. A., Khorana, H. G., and Hubbell, W. L. (1994) *Proc. Natl. Acad. Sci. U.S.A. 91*, 1667−1671.
47. Likhtenstein, G. I. (1974) in *Spin Labeling Methods in Molecular Biology* (Buchachenko, A. I., Ed.) pp 37−65, John Wiley & Sons, Toronto.
48. Eaton, G. R. and Eaton, S. S. (1989) in *Biological Magnetic Resonance 8: Spin Labeling, Theory and Applications* (Berliner, L. J., and Reuben, J., Eds.) pp 339−397, Plenum Press, New York and London.
49. Rabenstein, M. R., and Shin, Y. K. (1995) *Proc. Natl. Acad. Sci. U.S.A. 92*, 8239−8243.
50. Hustedt, E. J., Smirnov, A. I., Laub, C. F., Cobb, C. E., and Beth, A. (1997) *Biophys. J. 74*, 1861−1877.
51. Mchaourab, H., Lietzow, M. A., Hideg, K., and Hubbell, W. L. (1996) *Biochemistry 35*, 7692−7704.
52. Altenbach, C., Marti, A., Khorana, H. G., and Hubbell, W. L. (1990) *Science 248*, 1088−1092.
53. Zhan, H., Elliott, J. L., Shen, W. H., Huynh, P. D., Finkelstein, A., and Collier, R. J. (1999) *J. Membr. Biol. 167*, 173−181.

BI990520A